JOURNAL OF MATERIALS SCIENCE 27 (1992) 2035–2047

Damage in carbon fibre composites due to repetitive low-velocity impact loads

S. Y. GWEON, W. D. BASCOM
Department of Materials Science and Engineering, University of Utah, Salt Lake City, UT 84112, USA

The effect of repetitive impacting with increasing impact energy on unsupported thermoset matrix and thermoplastic matrix carbon fibre laminates was studied. In the case of the thermoset laminates, there were two abrupt losses in stiffness, the first corresponding to through-the-thickness damage and the second to the damage extending to the specimen edges. The thermoplastic matrix laminates exhibited a continuous decline in stiffness but again the damage sequence was through-the-thickness followed by extension to the specimen edges. Static bend testing of these composites resulted in the same type and extent of damage as was observed for impact loading. The effect of increasing the unsupported area and laminate thickness were investigated. Impacting with increasing impact energy was compared to repetitive impacting at a constant impact energy.

1. Introduction

The detrimental effects of low-velocity impacts on carbon fibre-reinforced polymer (CFRP) composites and the resultant loss in compression strength are well documented [1]. The majority of the research in this area has been on the effect of single impact events. The effect of repetitive fatigue impact loading has received less attention [2, 3]. One study [3] was of particular interest in that it was claimed that, by repetitive impacting with increasing impact energy, changes in the stiffness of the sample could be related to changes in the type of damage, i.e. delamination versus fibre breakage.

In the work reported here it is shown that these changes in specimen stiffness are the result of changes in the extent of damage rather than the type of damage and that the test is very dependent on specimen geometry and the matrix polymer. The repetitive impact with increasing impact energy (RIIE) test was still found to be useful for comparing the impact resistance of composites with different matrices, ply orientation and fibre type. It was also found that the RIIE test provides more information about the damage process than impact fatigue tests conducted at a constant impact load.

2. Experimental procedure

2.1. Materials

Four composite materials were studied, AS4/3501-6, IM6/3501-6 (an amine-cured tetrafunctional epoxy) and AS4/PEEK (polyetheretherketone). The dimensions and stacking sequence of the specimens tested are listed in Table I. The composite panels were fabricated from prepreg supplied by the indicated manufacturers and were processed into laminates according to the manufacturer's specifications. The specimens used in the impact tests were 5 cm × 8 cm or 10 cm × 13 cm coupons that had been cut from larger 15 cm × 15 cm panels.

2.2. Test conditions

The specimens were mounted on a fixture shown schematically in Fig. 1 such that 1.5 cm of the coupon was held by toggle clamps at each end leaving an unsupported area of 5 × 5 cm. A falling drop impact tester [4] was used which gave a computer readout of specimen displacement (stiffness) and transferred energy. The impactor weight was 1085 g and had a hemispherical tip with a diameter of 1.25 cm (0.5 in). The impact load was incremented by increasing the impactor height by 1 cm intervals over a range of 10–72 cm, the maximum height of the impact tower. Fatigue tests were done at a fixed height of 35 cm.

Static flexural tests were done using a three-point bending fixture on a servohydraulic machine (MTS 800). Post-impact tensile tests were done on the same machine at strain rates of 0.05 mm s^{-1}.

The undamaged panels were inspected using ultrasonic C-scanning to determine panel quality and then C-scanned after impacting to determine the extent of damage.

2.3. Sectioning and damage mapping

The impacted specimens were cut, potted in an epoxy resin, sectioned and polished for examination using light optics microscopy to determine the extent of damage. Damage maps were drawn using a three-dimensional plotting programme [5]. These techniques had been used in a previous study of impact

TABLE I Materials and panel configurations

Material	Panel dimensions			Stacking sequence
	Number of plies	Thickness (cm)	Unsupported area (cm^2)	
AS4/3501-6	32	0.435	100	$(0/90)_{8s}$
	32	0.435	25	$(0/90)_{8s}$ and $(\pm 45)_{8s}$
	16	0.230	25	$(0/90)_{8s}$
IM6/3501-6	32	0.435	25	$(0/90)_{8s}$ and $(\pm 45)_{8s}$
	16	0.240	25	$(0/90)_{8s}$
AS4/PEEK	32	0.416	100	$(0/90)_{8s}$
	32	0.416	25	$(0/90)_{8s}$ and $(\pm 45)_{8s}$

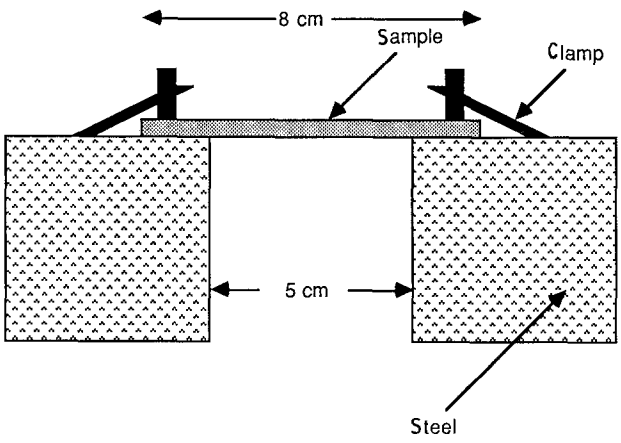

Figure 1 Clamping arrangement for impact specimens. An unsupported length of 10 cm was sometimes used.

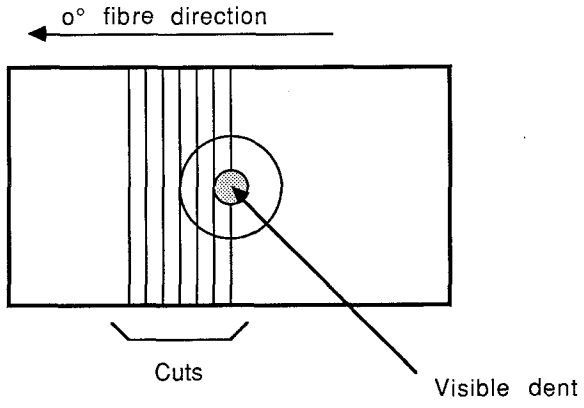

Figure 2 Schematic drawing of sectioning through the impact damage area.

damage [6] except that in the earlier work the damage maps had been drawn manually.

The cutting and slicing procedures are shown in Fig. 2. The damage region determined from C-scanning was cut and then embedded in a clear, room-temperature curing epoxy consisting of a mixture of a diglycidylether Bisphenol A epoxide (Epon 828), a polyamine curative (Jeffamine 230) and an accelerator (Texaco 399) at a weight ratio of 10:5:1, respectively. One-half of the potted sample was then sectioned from the point of impact indicated by a small dent in the panel surface. One face of each section was then polished on a metallographic polishing wheel using, in sequence, nos 320 and 400 grit papers followed by wet polishing with 3 and 1 μm Al_2O_3 aqueous pastes on a velvet cloth. The final thickness of the sections after polishing was 1.9 mm. The polished surfaces were examined using reflected light microscopy for the type and extent of damage in each ply. Maps of the damaged region were then drawn to indicate the extent of damage in each ply through the thickness of the laminate.

3. Results

3.1. AS4/3501-6 $(0/90)_{8s}$

The change in stiffness with increasing cumulative impact energy is plotted in Fig. 3. The stiffness was calculated from the maximum force divided by the maximum deflection and also from the impact time, i.e. the stiffness, k, from the mass-spring model is given by

$$k = m\pi^2/t^2 \quad (1)$$

where m is the total mass (impactor plus sample) and t the impact time. In the plots of stiffness versus cumulative impact energy, the open data points were obtained from the maximum force/maximum energy and the solid data points were obtained from Equation 1.

The per cent transferred energy versus cumulative impact energy is shown in Fig. 4. Transferred energy

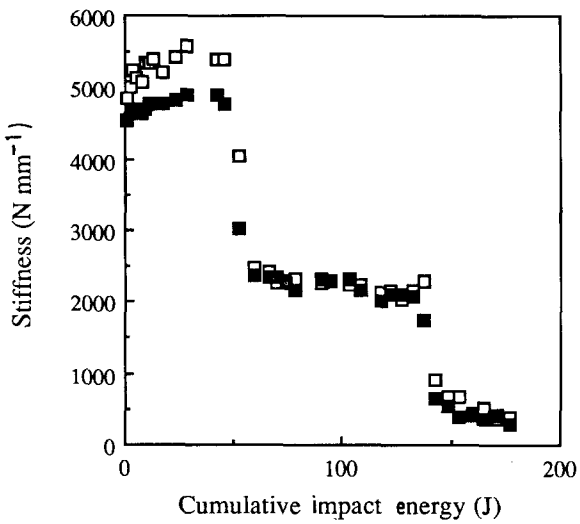

Figure 3 Stiffness versus cumulative impact energy, AS4/3501-6 $(0/90)_{8s}$.

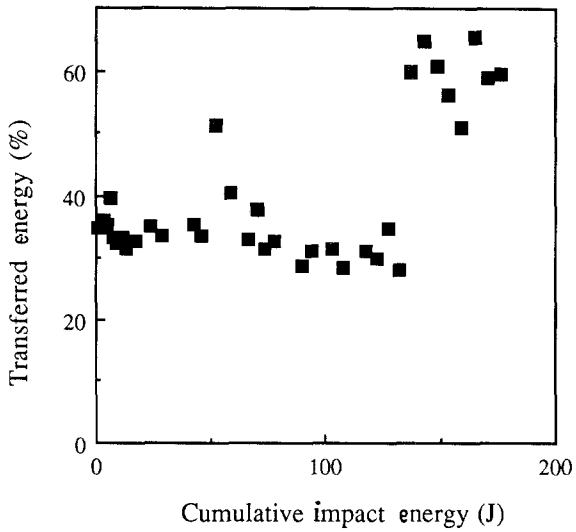

Figure 4 Per cent transferred energy versus cumulative impact energy, AS4/3501-6 $(0/90)_{8s}$.

was obtained by subtracting the energy of the impactor at the end of the impact event from the initial energy of the impactor.

In the plot of stiffness versus cumulative energy, three distinct stages of more or less constant stiffness were found at ~ 5200, ~ 2100 and $\sim 630\ N\,mm^{-1}$. The transferred energy was relatively constant through the first two stages except for a peak value between the first and second stage. During the final stage, the transferred energy was very erratic with large variations between impacts.

C-scans were taken of specimens that had been impacted to about the mid-point of each of the three stages of stiffness shown in Fig. 3. These same specimens were then sectioned and damage maps generated. The C-scans are shown in Fig. 5 and the damage maps in Fig. 6. After a cumulative impact energy of 10 J the C-scan indicated only a narrow damage area (Fig. 5a) and from Fig. 6a the damage was limited to the first few top plys. After 80 J cumulative impact energy, which is beyond the first drop in stiffness (Fig. 3), the C-scan indicated a wider damage area (Fig. 5b) that, extended through the thickness of the laminate (Fig. 6b). After 170 J cumulative impact energy, the C-scan (Fig. 5c) and the damage map (Fig. 6c) indicated that damage had extended to the edges of the laminate.

3.2. AS4/3501-6 $(\pm 45)_{8s}$

The impact response of laminates with fibre orientations of $\pm 45°$ in the 3501-6 matrix were similar to the observations with the 0°/90° fibre orientation. As shown in Fig. 7, three regions of relatively constant stiffness were found and the transferred energy exhibited a spike at the transition between the first drop off in stiffness and erratic behaviour after the second transition (Fig. 8). The only differences between the 0/90 and the ± 45 laminates was that the second stage of stiffness versus cumulative energy extended to higher energies for the ± 45 laminate and the third stage was not as clearly defined as in the case of the 0/90 laminate.

Damage maps of the second stage again indicated through-the-thickness damage (Fig. 9a) and that in the third stage the damage extended to the edges of the laminate (Fig. 9b).

3.3. IM6/3501-6 $(0/90)_{8s}$ and IM6/3501-6 $(\pm 45)_{8s}$

The stiffness and per cent transferred energy versus cumulative impact energy for IM6/3501-6 (0/90) and IM6/3501-6 (± 45) are presented in Figs 10 and 11, respectively. Three distinct slopes were observed in the stiffness plots for the IM6/3501-6 (0/90) laminate (Fig. 10a) and, as with the AS4 laminates, the second and third stage correspond to through-the-thickness damage and extension of the damage to the edges of the sample as indicated in the damage maps presented in Fig. 12.

The change in stiffness and the per cent transferred energy results for the IM6/3501-6 (± 45) are presented in Fig. 11. As in the case of the AS4 laminates, the second stage extended to higher cumulative impact energies than for the (0/90) laminates and, in fact, we were unable to identify a third stage due to the upper limit of the impact test equipment.

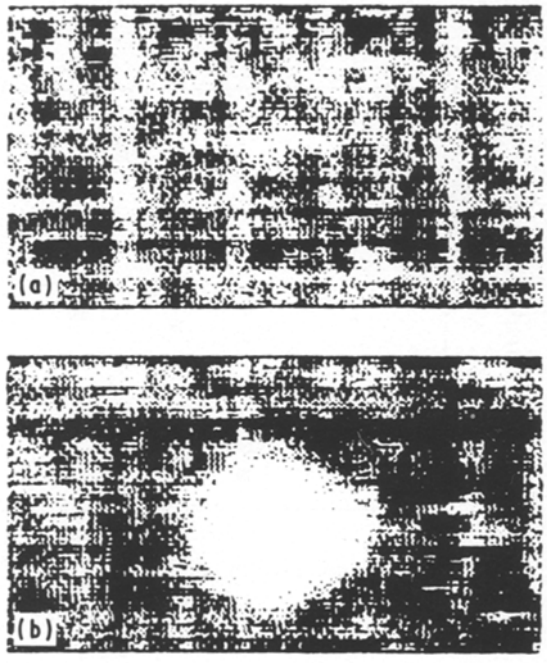

Figure 5 C-scans of impact damage of AS4/3501-6 $(0/90)_{8s}$ after cumulative impact energies (ΣIE) of (a) 10 J, (b) 80 J and (c) 170 J.

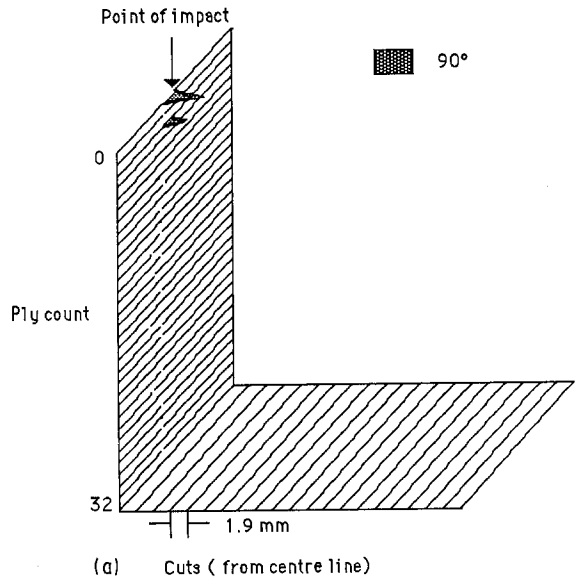

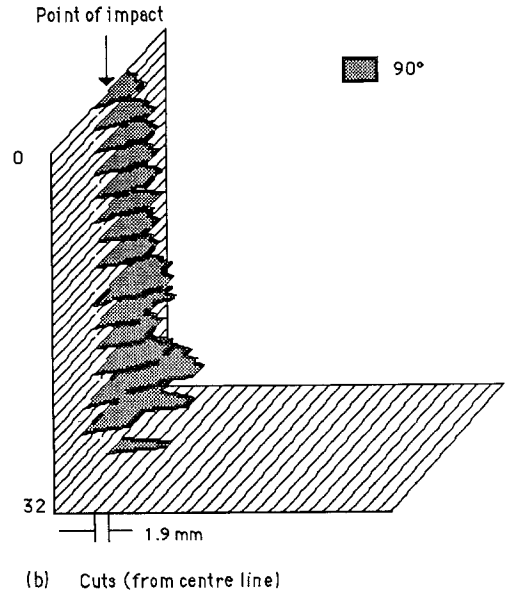

Figure 6 Damage maps of AS4/3501-6, $(90/0)_{8s}$ after ΣIE of (a) 10 J, (b) 80 J and (c) 170 J.

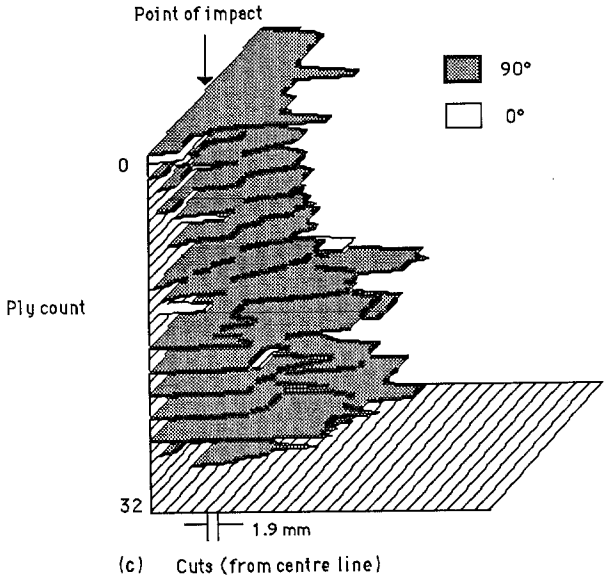

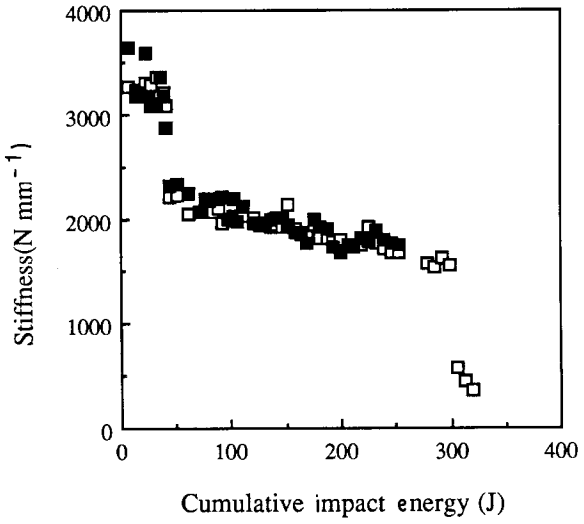

Figure 7 Stiffness versus cumulative impact energy AS/4 (± 45)$_{8s}$.

3.4. AS4/PEEK $(0/90)_{8s}$

Fig. 13 shows the change in stiffness and per cent transferred energy versus cumulative impact energy for an AS4/PEEK $(0/90)_{8s}$ laminate. Unlike the results for the 3501-6 matrix materials, there were no distinct stages or plateaus of constant stiffness. Instead, the stiffness was relatively constant up to about a cumulative impact energy of 100 J at which point there was a more or less continuous decrease in stiffness. The per cent transferred energy was relatively constant up to the point where the stiffness began to decrease beyond which the transferred energy became erratic.

The C-scans of this laminate after different cumulative impact energies are shown in Fig. 14 and the corresponding damage maps in Fig. 15. Up to about 35 J the damage is relatively minor and confined to the first few top plys and to the back outer ply. At a cumulative energy of 155 J, at which point the stiffness was beginning to decrease, more extensive damage was observed as shown in the damage map (Fig. 15b) and at 280 J the damage extended to the specimen edges (Fig. 15c). None the less, the extent of damage

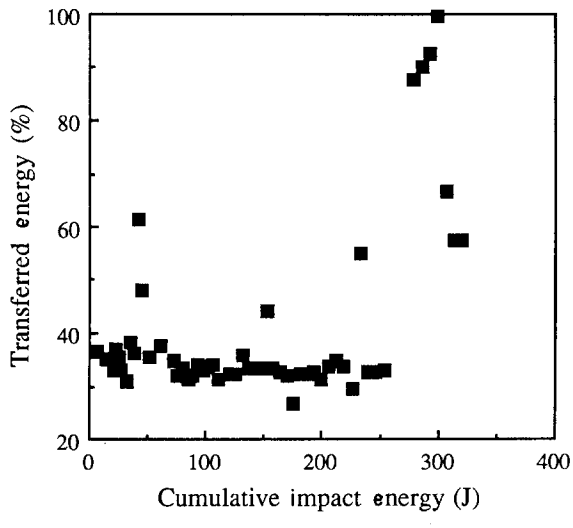

Figure 8 Per cent transferred energy versus cumulative impact energy, AS4/3501-6 (± 45)$_{8s}$.

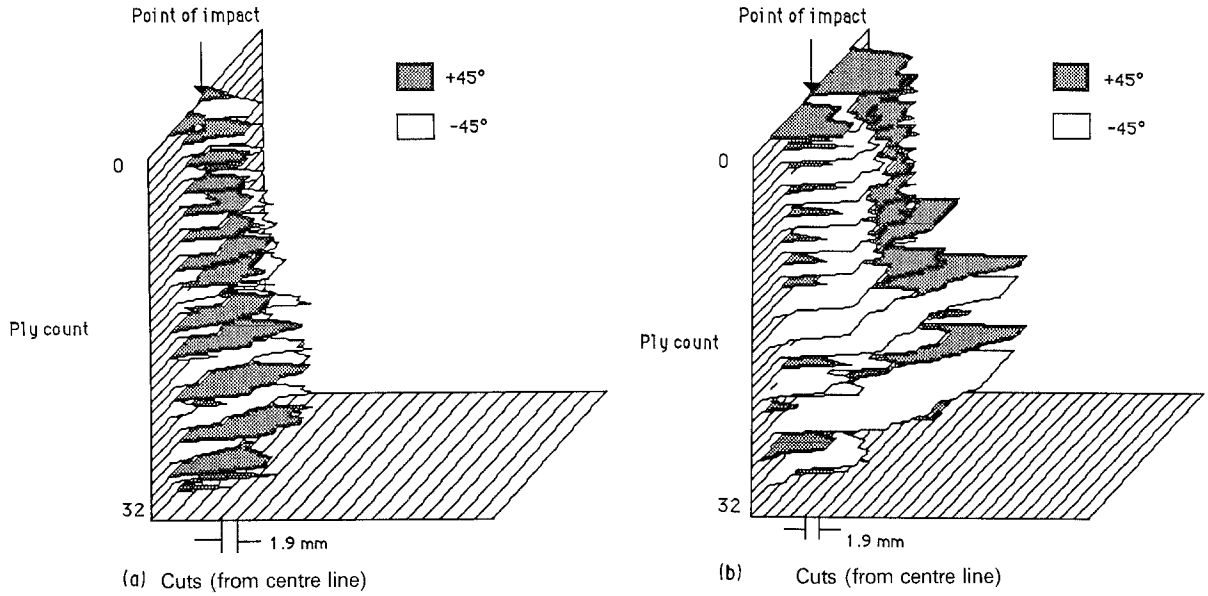

Figure 9 Damage maps of AS4/3501-6 ($\pm$ 45) after ΣIE of (a) 80 J and (b) 31 J.

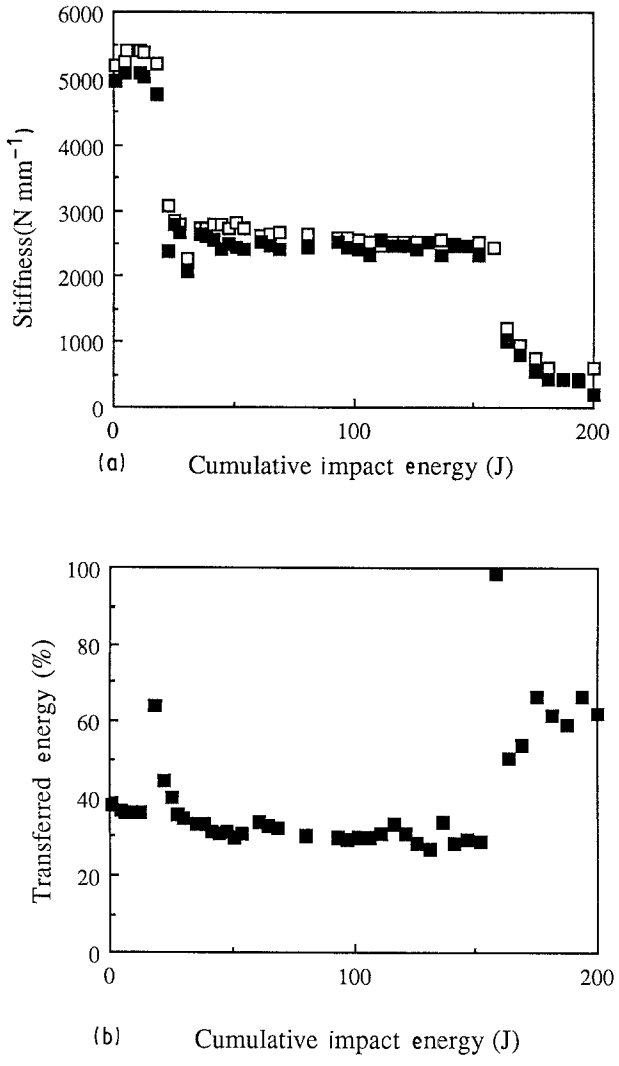

Figure 10 (a) Stiffness and (b) per cent transferred energy versus cumulative impact energy for IM6/3501-6 $(0/90)_{8s}$.

was significantly less than for the brittle 3501-6 laminates; compare Figs 6c and 15c. However, in the case of the AS4/PEEK laminates extensive fibre damage was observed as shown in Fig. 16.

3.5. AS4/PEEK $(\pm 45)_{8s}$

Impacting did not alter the stiffness of this ($\pm$ 45) laminate until the cumulative energy reached 150 J (Fig. 17a) whereas the drop-off in stiffness occurred at 100 J in the case of the (0/90) laminate. Again, this loss in stiffness was accompanied by an erratic variation in transferred energy (Fig. 17b). A C-scan at a cumulative energy of 250 J is shown in Fig. 18 and the corresponding damage map in Fig. 19.

3.6. Effect of coupon dimensions and thickness

In these experiments the effect of specimen dimensions was studied by increasing the unsupported area from 25 cm^2 (5 cm $\times$ 5 cm) to 100 cm^2 (10 cm $\times$ 10 cm). The effect of sample thickness was studied by reducing the number of plys from 32 to 16.

The effect of changing the unsupported area is shown in Figs 20 and 21 for AS4/3401-6 and AS4/PEEK, respectively. As might be expected, the increase in area allows more energy dissipation by elastic bending so that the coupons with unsupported dimensions of 10 cm $\times$ 10 cm did not exhibit significant changes in stiffness compared to the 5 cm $\times$ 5 cm specimens.

Decreasing the laminate thickness resulted in the onset of damage at a lower cumulative impact energy. As shown in Fig. 22, the 16-ply laminate of AS4/3501-6 exhibited an initial drop in modulus after the first impact (1.5 J) and then at about 25 J. The first drop in stiffness for the 32-ply laminate was at about 50 J. A damage map for the 16-ply laminate after a cumulative impact energy of 10 J is shown in Fig. 23 and it is evident that damage had extended through the laminate thickness.

3.7. Fatigue testing at constant impact energy versus increasing impact energy

Coupons of AS4/3501-6, $(0/90)_{8s}$ were tested in a

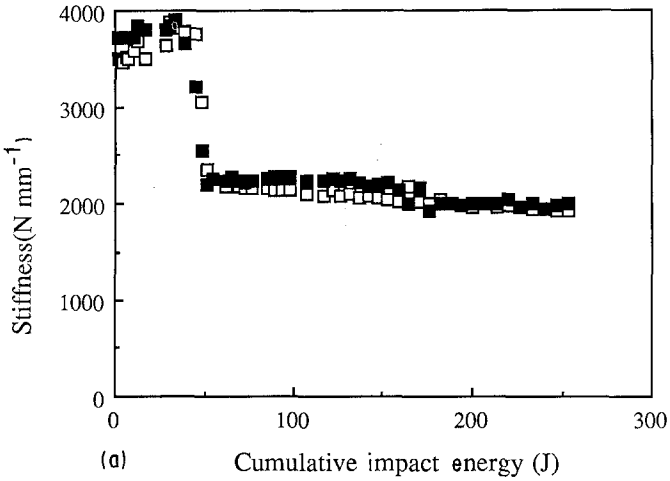

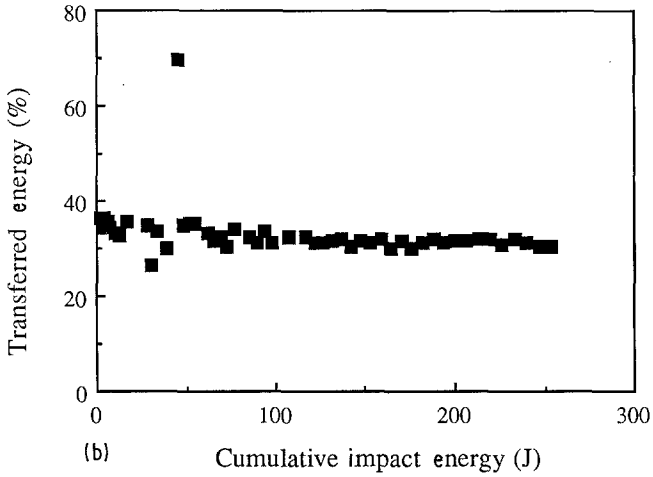

Figure 11 (a) Stiffness and (b) per cent transferred energy versus cumulative impact energy for IM6/3501-6 ($\pm$ 45)$_{8s}$.

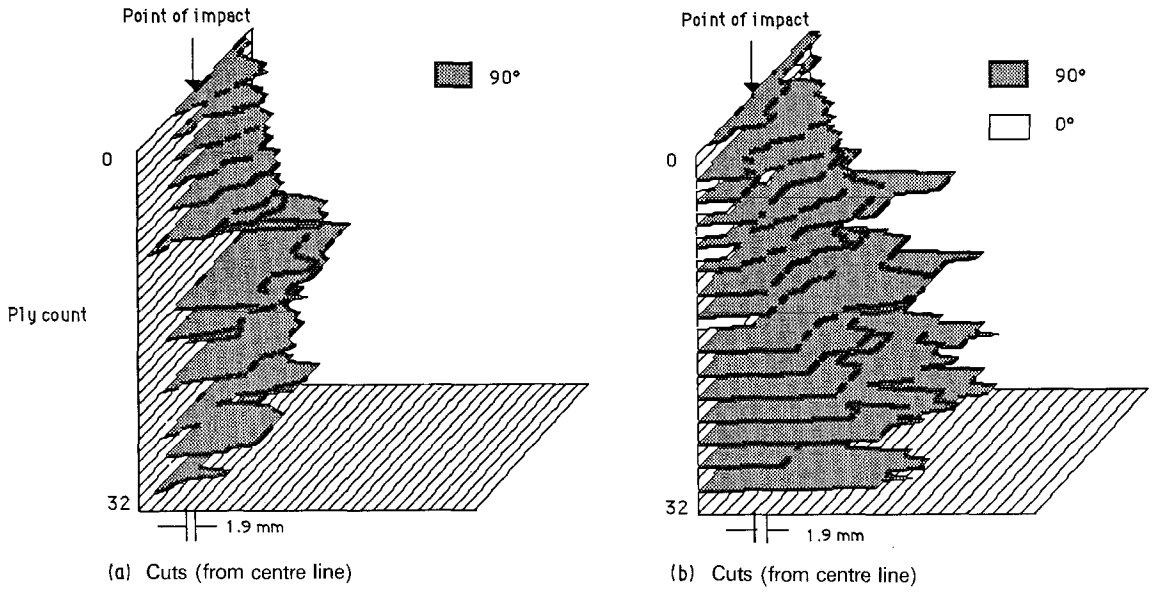

Figure 12 Damage maps for IM7/3501-6 (0/90)$_{8s}$ after ΣIE of (a) 110 J and (b) 190 J.

"conventional" fatigue mode where the specimens were repetitively impacted at a constant impact load. The results are compared with impacting with increasing impact load in Fig. 24. In the fatigue mode there is an initial drop in stiffness but with no subsequent change even up to a cumulative impact energy of 400 J. The repetitive impacting with increasing impact energy resulted in a second decline in stiffness at a cumulative energy of about 150 J.

These data for increasing impact energy are presented in terms of the actual impact energy rather than the cumulative impact energy in Fig. 25. The initial drop in stiffness occurs at about 3 J. In Fig. 24, the initial drop in stiffness for impacting at constant en-

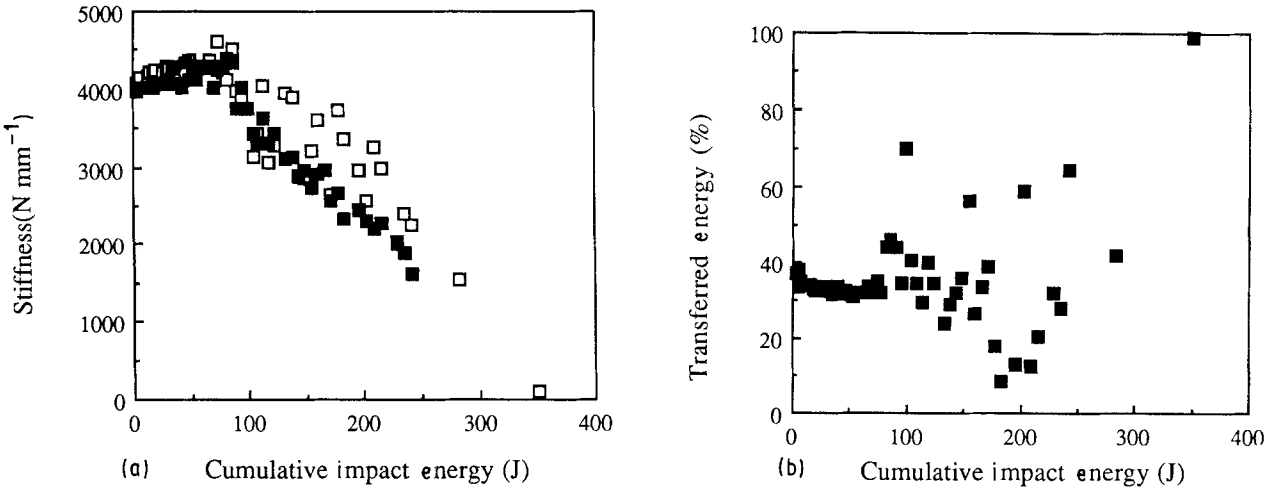

Figure 13 (a) Stiffness and (b) per cent transferred energy versus cumulative impact energy for AS4/PEEK $(0/90)_{8s}$.

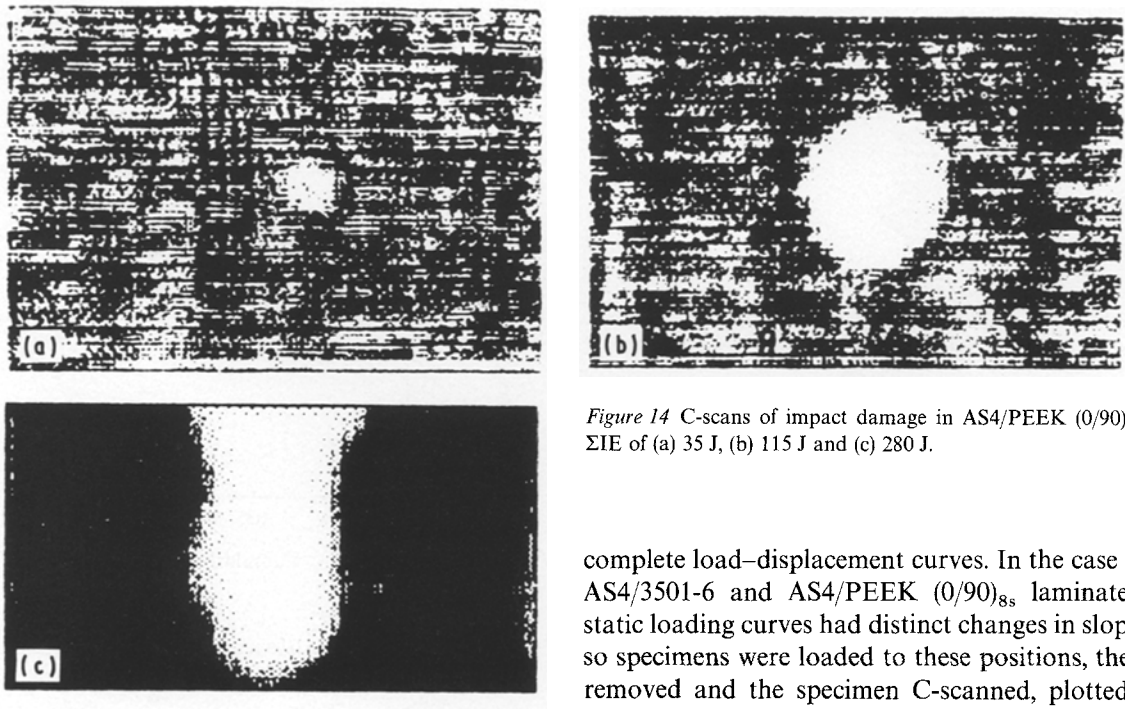

Figure 14 C-scans of impact damage in AS4/PEEK $(0/90)_{8s}$ after ΣIE of (a) 35 J, (b) 115 J and (c) 280 J.

ergy occurred at 3 J. It would appear that there is a threshold impact energy for through-the-thickness damage that is arrived at whether the test is a fatigue test at constant impact energy or by incrementally increasing the impact energy. However, by holding the impact energy constant the next phase of damage, extension of the damage to the specimen edges, may not be realized.

3.8. Static loading

A comparison was made between dynamic impact loading and static three-point flexure loading. The strain rate of the static test was 0.05 mm s^{-1}. The loading pin was hemispherical with a tip having the same diameter as the impact loader (0.5 in) and the specimens were supported identically as in the dynamic tests, i.e. 5 cm × 5 cm unsupported area. Initially the specimens were loaded to failure to establish complete load–displacement curves. In the case of the AS4/3501-6 and AS4/PEEK $(0/90)_{8s}$ laminates the static loading curves had distinct changes in slope and so specimens were loaded to these positions, the load removed and the specimen C-scanned, plotted, sectioned and observation of the sections used to construct damage maps.

Three distinct regions were observed in the static tests of AS4/3501-6 $(0/90)_{8s}$ as shown in Fig. 26. In the first region, the stiffness was 5000 N mm^{-1} with an abrupt decrease to 2300 N mm^{-1} followed by a second drop in stiffness to about 500 N mm^{-1}. These changes in stiffness are quantitatively similar to the changes in stiffness observed in the dynamic impact tests (Fig. 3).

Damage maps were constructed at displacements of ~ 3 and ~ 4 mm and are presented in Fig. 27. No damage was observed at a displacement of 1.5 mm. As in the case of impact loading, the initial damage was through-the-thickness followed by extension of the damage to the specimen edges. Fibre breakage was observed on the back surface of the laminate displaced to 4 mm whereas for the impacted specimen, fibre breaks were observed in the front surface plies. Both the statically loaded and the impacted specimens showed a similar conical damage distribution through the specimen thickness, e.g. compare Figs 6b and 27a.

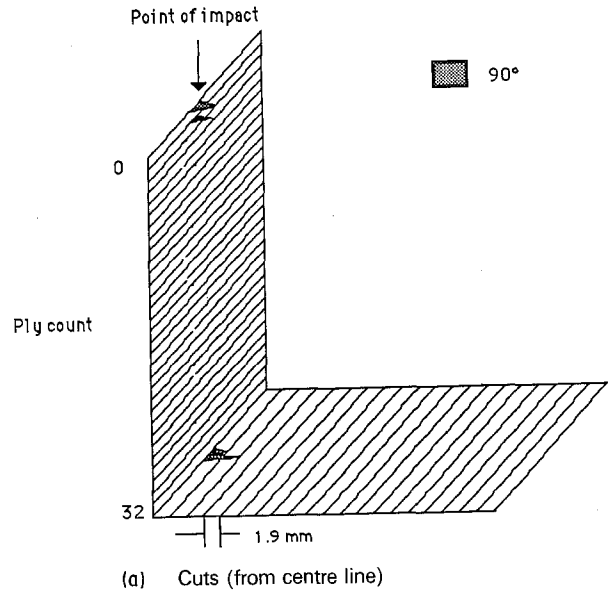

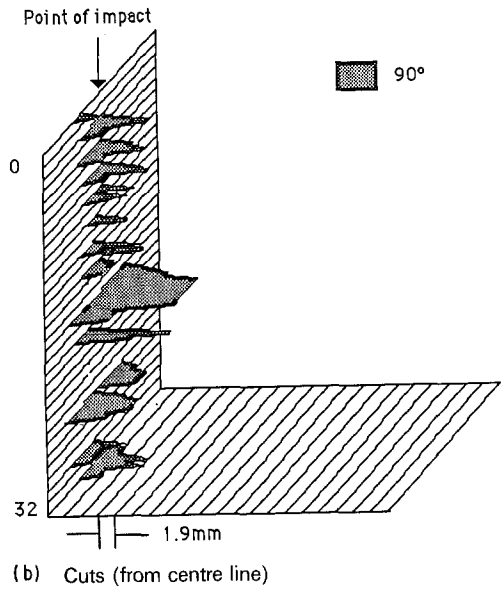

Figure 15 Damage maps of AS4/PEEK $(0/90)_{8s}$ after ΣIE of (a) 35 J, (b) 115 J and (c) 200 J.

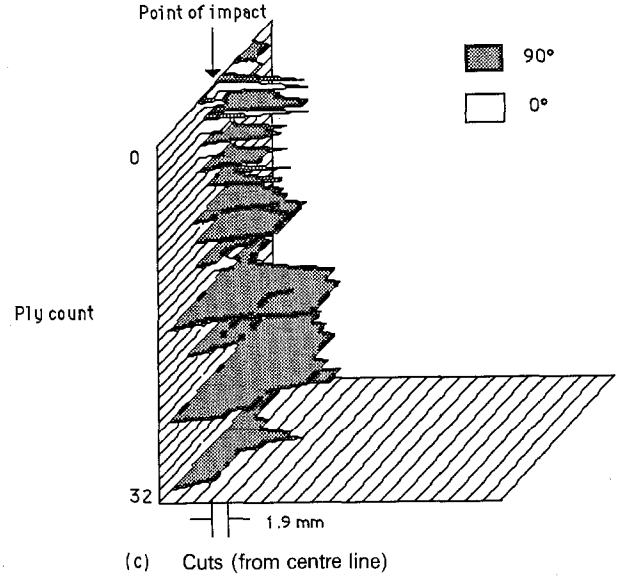

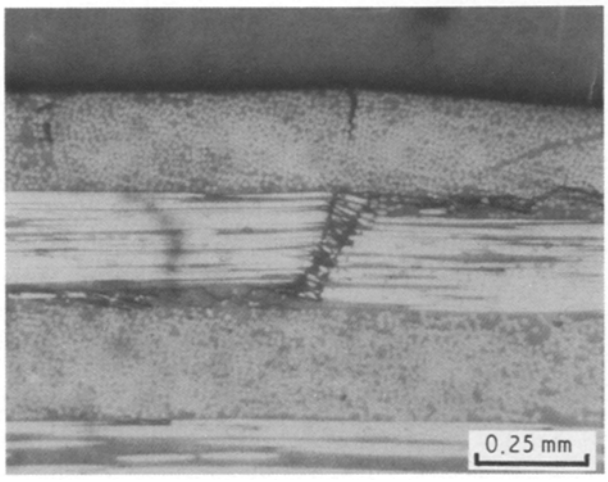

Figure 16 Photomicrograph of fibre breakage in AS4/PEEK $(0/90)_{8s}$ after ΣIE of 115 J.

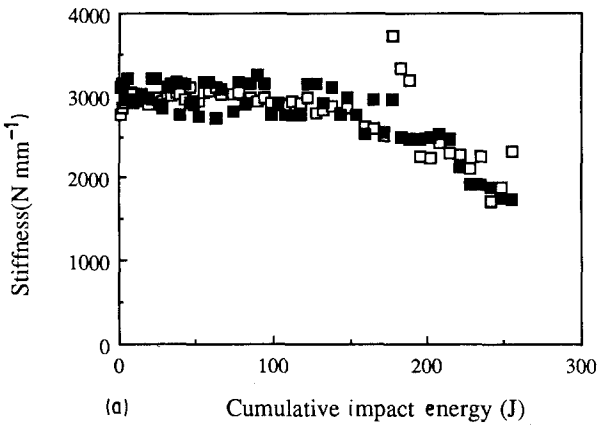

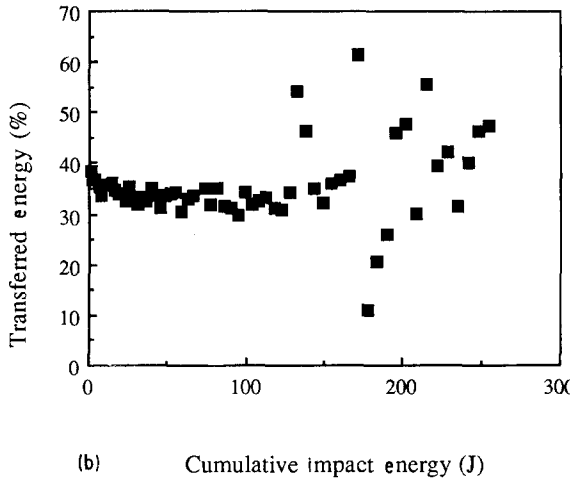

Figure 17 (a) Stiffness and (b) per cent transferred energy for AS4/PEEK $(\pm 45)_{8s}$.

The static flexure load–displacement curve for AS4/PEEK $(0/90)_{8s}$ is presented in Fig. 28. The initial slope (stiffness) was more or less constant but then went through a broad maximum at about 4–4.5 mm displacement beyond which the stiffness decreased abruptly. The initial stiffness in the case of the PEEK matrix laminate was $\sim 3500\ N\,mm^{-1}$ compared to $\sim 4300\ N\,mm^{-1}$ measured in the impact test. Speci-

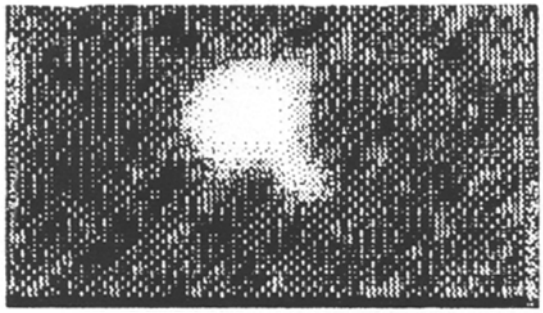

Figure 18 C-scan of impact damage of AS4/PEEK, (± 45) at ΣIE of 250 J.

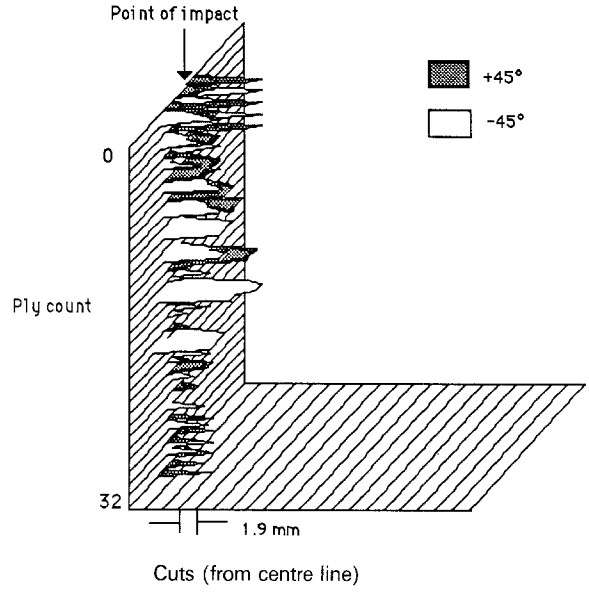

Figure 19 Damage map of AS4/PEEK (± 45)$_{8s}$ after ΣIE of 250 J.

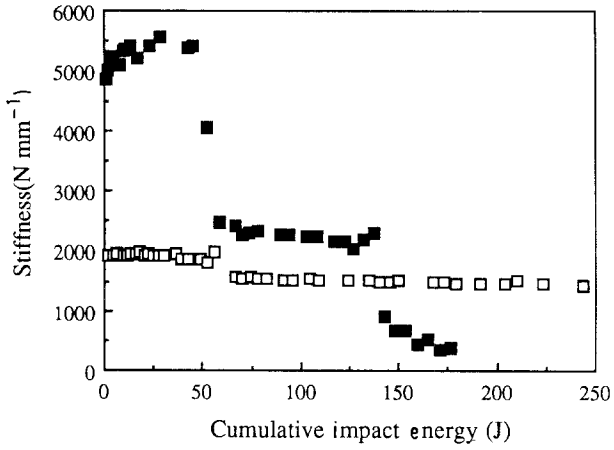

Figure 20 Comparison of stiffness versus cumulative impact energy for AS4/3501-6 (0/90)$_{8s}$ having unsupported dimensions of (■) 5 cm × 5 cm and (□) 10 cm × 10 cm.

mens were loaded to displacements of 2.5, 4 and 5.5 mm, sectioned and inspected for damage. No damage was observed at 2.5 mm, and only minor damage in the front and back surface plies at 4 mm, although there was a noticeable bulge on the back surface. A damage map is shown for the specimen displaced to 5.5 mm in Fig. 29.

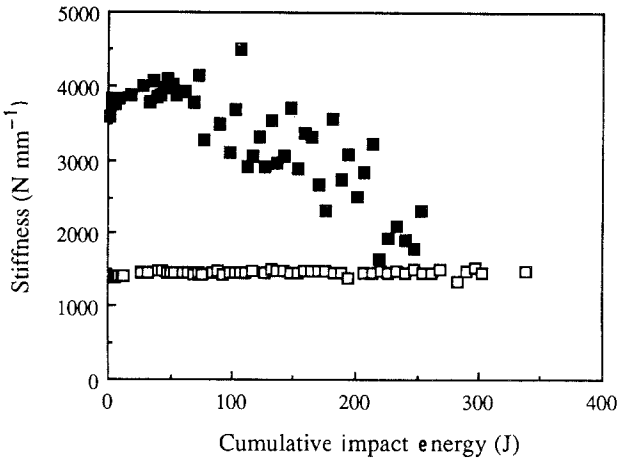

Figure 21 Comparison of stiffness versus cumulative impact energy for AS4/PEEK (0/90)$_{8s}$ having unsupported dimensions of (■) 5 cm × 5 cm and (□) 10 cm × 10 cm.

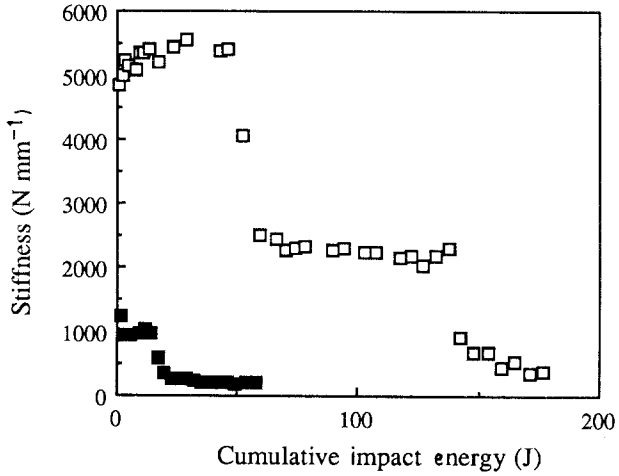

Figure 22 Comparison of stiffness versus cumulative impact energy for AS4/3501-6 (0/90) laminates having (■) 16 and (□) 32 plys.

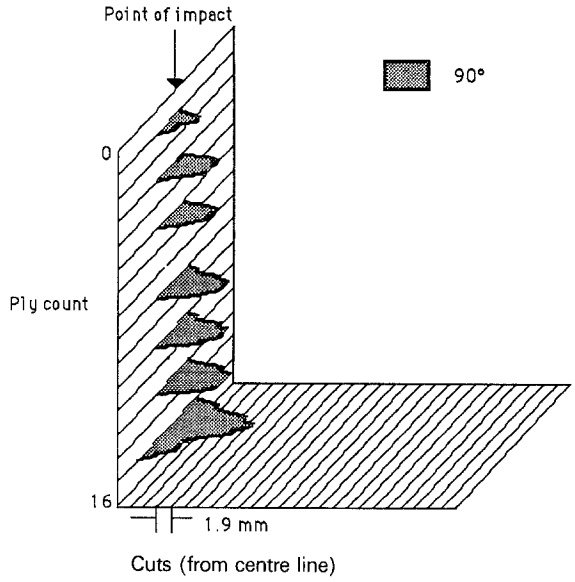

Figure 23 Damage map for AS4/3501-6 (90/0)$_{4s}$ at ΣIE of 10 J.

3.9. Post-impact tensile modulus

Specimens were impacted to cumulative impact energies that were known to result in (a) minimal damage, (b) through-the-thickness damage, and (c) where dam-

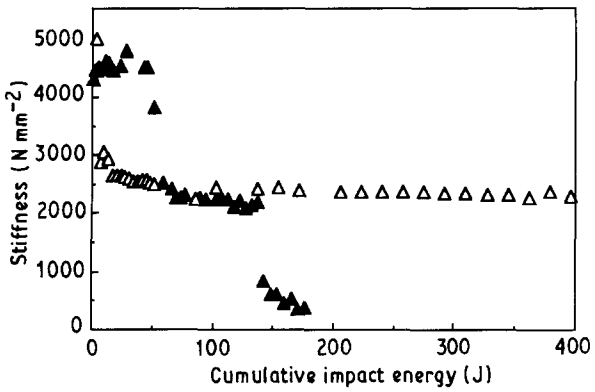

Figure 24 Comparison of the change in stiffness versus cumulative impact energy for fatigue loading at (Δ) constant and (▲) increasing impact energy for AS4/3501-6 $(0/90)_{8s}$.

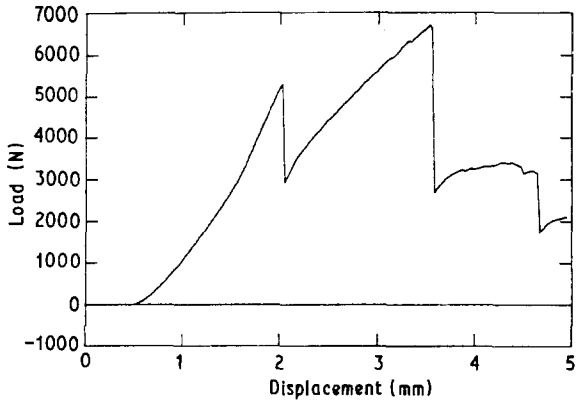

Figure 26 Static flexure load–displacement plot for AS4/3501-6 $(0/90)_{8s}$.

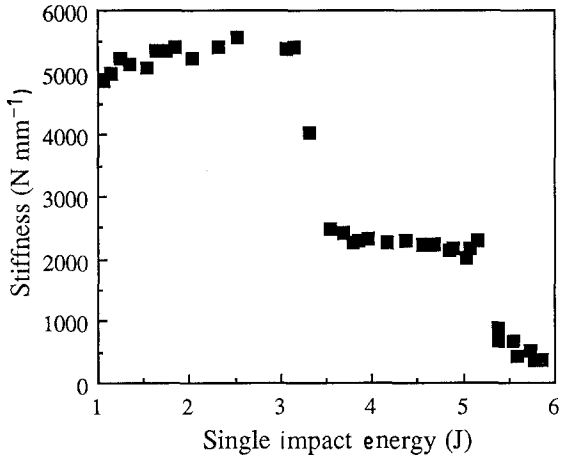

Figure 25 Stiffness versus single impact energy for AS4/3501-6, $(0/90)_{8s}$.

age had extended to the specimen edges. Each specimen was tested for tensile modulus. In all cases the laminate orientation was $(0/90)_{8s}$. The results are presented in Fig. 30. Initially, the 3501-6 laminate with the IM fibre had a higher modulus than the corresponding laminate with the AS fibre, as expected. However, after a cumulative impact energy of over 200 J, the moduli were essentially the same, suggesting that the damage was so severe that it was determined primarily by the matrix, i.e. fibre fracture was so extensive that they were unable to carry load. On the other hand, the tensile modulus of the PEEK laminate was essentially unchanged up to about 275 J, despite the fact that this laminate had also suffered fibre breakage.

4. Discussion

The general sequence of damage with increasing impact energy proceeded from an initial stage through which only minor damage occurred (transverse and delaminations notable in the front and back side plys) and no decrease in stiffness. This initial stage was then followed by through-the-thickness damage and a major decrease in stiffness. Subsequently, the damage reached the edges of the laminate accompanied by a

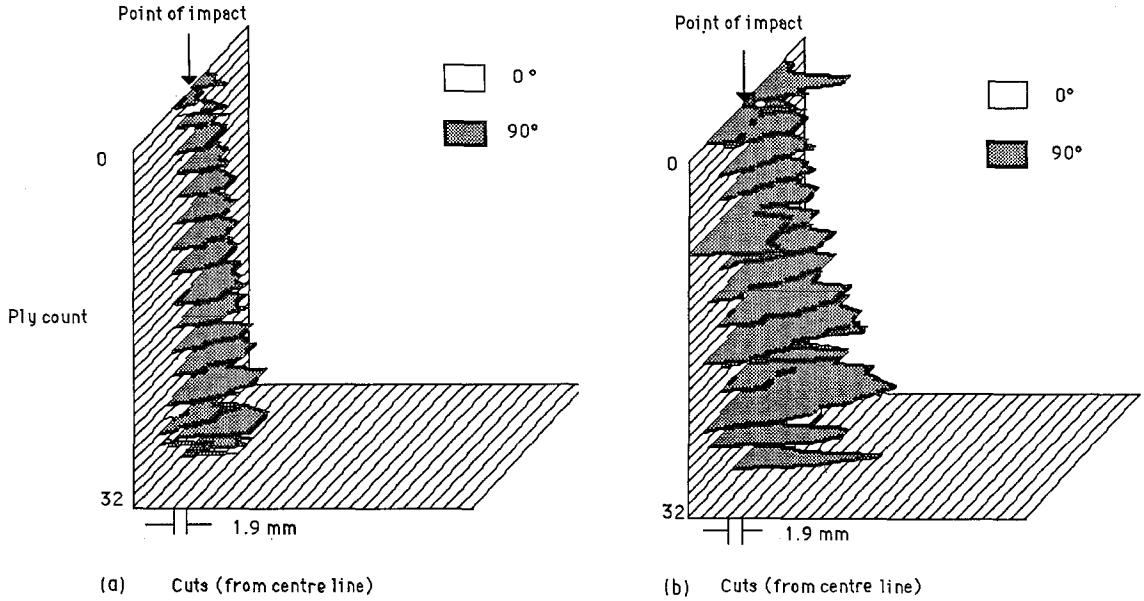

Figure 27 Damage map of AS4/3501-6 $(90/0)_{8s}$ static loaded to a displacement of (a) ~ 3 mm and (b) 4 mm.

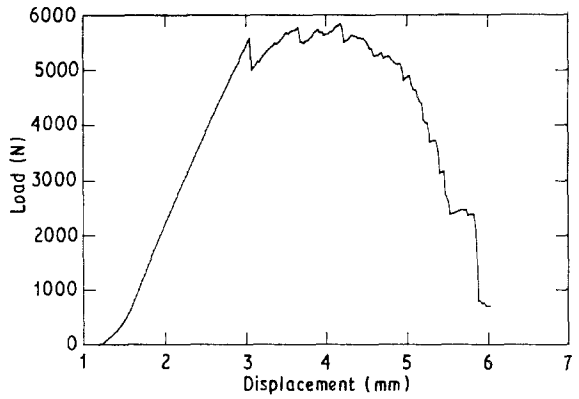

Figure 28 Static flexure load–displacement curve for AS4/PEEK $(0/90)_{8s}$.

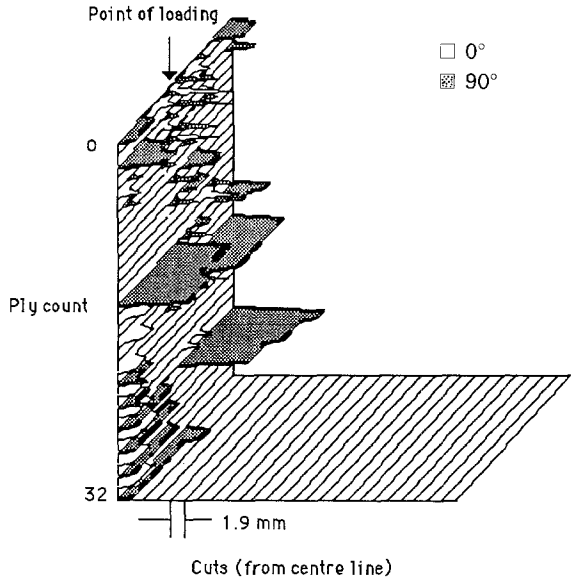

Figure 29 Damage map of AS4/PEEK $(90/0)_{8s}$ static loaded to a displacement of ~ 5.5 mm.

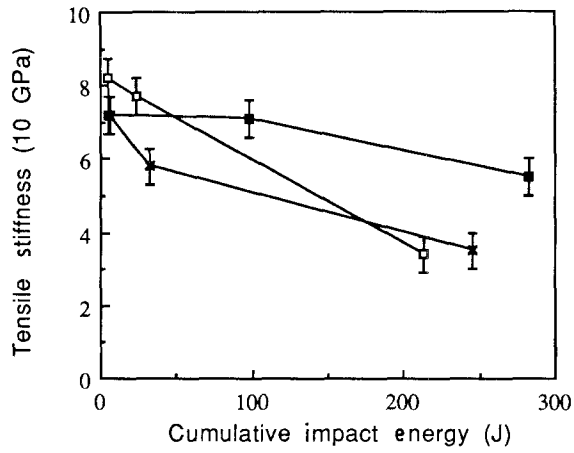

Figure 30 Tensile modulus versus cumulative impact energy. All laminates were $(0/90)_{8s}$. (×) AS4/3501-6, (□) IM6/3501-6, (■) AS4/PEEK.

further loss in stiffness. In the case of the brittle 3501-6 matrix materials these changes were abrupt while in the case of the much tougher PEEK matrix laminate the change in stiffness was gradual.

Actually, a slight increase in stiffness was observed during the initial stage; see Figs 3, 10, 11 and 13. This same effect was observed in the static flexural tests. Note the change in the initial slope in Figs 26 and 28. The reason for the stiffness increase is not immediately obvious. It may be due to microcracking in resin-rich regions which would effectively transfer load bearing from these low-modulus regions to adjacent high-modulus fibres.

Extension of the damage through the laminate thickness in effect resulted in a "hole" through the laminate. In the case of the brittle matrix composites, there was an abrupt drop in stiffness accompanied by a peak in the transferred energy and an audible click. At this stage the laminate stiffness is determined by the undamaged ligaments between the "hole" and the specimen edges. Subsequent impacting would presumably increase the damage area, thereby shortening the ligament width. However, if the damage area is increasing it is not obvious why the laminate stiffness should be relatively constant. There are at least two explanations for this observation: first, that the area of damage does not increase significantly but that the impact energy is dissipated by multiple transverse and longitudinal cracking until a point is reached where the only way energy can be further dissipated is by damage being extended away from the central area; secondly, that the damage area is not equivalent to a hole through the laminate but in fact has residual stiffness and that this stiffness is not significantly effected by the widening of the damage area. The latter argument is supported by the fact that, in brittle matrix composites, impact damage is largely matrix cracking with relatively little fibre fracture. As the damage extends laterally, the stiffness is determined by the intact fibres.

In the case of the thermoplastic matrix composite, the decline in stiffness is continuous. It has been shown [6] that, due to the high resistance to transverse and interlaminar matrix fracture, energy adsorption involves extensive fibre fracture. Therefore, unlike the brittle matrix composites, extension of the through-the-thickness damage involves fibre breakage and a loss in stiffness.

Once the damage area reaches the specimen edges, the laminate responds much like a coupon with a weak central hinge. It is not at all surprising that there is an abrupt drop in stiffness which can be as much as four to five orders of magnitude lower than the undamaged laminate.

Changes in the specimen dimensions had profound effects on the impact damage and the change in laminate stiffness. These effects are not at all surprising. Any change in specimen dimensions that alters the elastic adsorption of energy will dramatically effect the impact response. Increasing the unsupported area from 25 cm^2 to 100 cm^2 resulted in the impact energy being dissipated by elastic deformation with a nearly total reduction of irreversible damage (Figs 20 and 21). Conversely, reducing the laminate thickness resulted in the onset of irreversible damage at lower impact energies. In this case there is less material available for elastic deformation.

The change in transferred energy with cumulative impact energy resulted in some curious results. The transition to through-the-thickness damage was usually accompanied by a peak in the transferred energy in the case of the brittle matrix composites. Once the damage reached the specimen edges, the transferred energy became erratic with wide variations from one impact event to the next.

If we view this variation in transferred energy as a change in the resilience of the laminate to impact loading then the peak observed at the onset of through-the-thickness damage is reasonable if the damage does not immediately extend beyond the initial damage area as suggested above. Once the damage extended to the specimen edges the transferred energy became erratic. We can only speculate that, from one impact event to the next, the orientation of fibres and matrix cracking resulted in configurations that varied in their capacity to adsorb impact energy.

The RIIE test differs from the simple fatigue test, in that the impact energy is increased incrementally in the RIIE test, whereas in the fatigue test the energy is constant for each successive impact. The fatigue study was done using an impact energy of 3.2 J and after the first impact the laminate stiffness was reduced from about 5000 $N mm^{-1}$ to about 2000 $N mm^{-1}$. In the RIIE test the cumulative energy reached 100 J before the stiffness dropped from 5000–2000 $N mm^{-1}$ (Fig. 24). Replotting the RIIE data to show the actual impact energy (Fig. 25) shows that the first decline in stiffness occurred at about 3 J. It would appear that some specific damage condition (through-the-thickness damage) occurs at this impact energy level.

Continuing the fatigue test at a constant 3 J for each impact resulted in no further change in stiffness. On the other hand, continuation of the RIIE test, results in a second change in stiffness at about 5 J (Fig. 25). Here again, a change in the extent of damage, through-the-thickness to extension to the laminate edges, depends on the level of impact loading rather than the cumulative impact energy.

The effect of the two stacking orientations, (0/90) and ($\pm$ 45), were similar for all of the laminate materials. As expected, the initial stiffnesses for the ($\pm$ 45) orientations were always lower than that of the (0/90) orientations. As the stiffness began to decrease, the ($\pm$ 45) laminates showed more resistance to damage propagation than the (0/90) laminates. Evidently the $\pm$ 45 stacking sequence can absorb larger amounts of impact energy than 0/90 stacking sequence by elastic shear deformation; an elastic, "scissoring" deformation.

For the 3501-6 matrix laminates, the static tests gave very similar results to those of the dynamic tests. Three distinct stiffness regions were found in the three-point bending tests and the stiffness values from the static tests and dynamic tests were nearly identical. In addition, the extent of damage and the type of damage, transverse and longitudinal cracking and fibre breakage, at each stage were similar for the static and dynamic tests.

On the other hand, the stiffnesses of the PEEK matrix laminates in the static tests were lower than from the impact testing and the damage modes were also different. These differences can be interpreted in two ways. One is membrane deformation and the other is viscoelastic behaviour. In ductile materials, deflection in the static test occurs not only by contact and bending deformation but also by membrane deformation, especially in a plate supported at two edges. The fact that membrane deformation was involved in the PEEK composite is evident from the damage maps. In the impact test, damage was confined to the region below the point of impact (Fig. 15). In the static test, large amounts of damage were found out to the edges of the sample (Fig. 29).

The other explanation for the differences in stiffness is the viscoelastic characteristic of the thermoplastic. At the low strain rate of the static test (0.05 $mm s^{-1}$) the laminate exhibits a lower stiffness than at the high strain rate impact loading.

The post-impact tensile modulus results (Fig. 31) are, at first glance, somewhat surprising. One would have thought that delamination and transverse cracking, which dominate the impact response of the 3501-6 laminates, would be less severe on tensile stiffness than the fibre breakage sustained by the PEEK laminate. In fact, the PEEK laminate suffered less reduction in modulus than the AS4/3501-6 and the IM6/3501-6 laminates. It would appear that the extent of damage rather than the type of damage is more important in this post-impact test.

The specimen geometry effects on the extent of damage were as expected. Increasing the unsupported area from 25 cm^2 (5 cm $\times$ 5 cm) to 100 cm^2 (10 cm $\times$ 10 cm) allows for more energy to be dissipated by elastic flexure. Decreasing the laminate thickness from 32 plies to 16 plies (at the same unsupported area, 25 cm^2) reduces the amount of material available to resist impact loads by elastic deformation.

The RIIE test is useful in that it is sensitive to the effect of matrix, fibre type and fibre orientation on damage tolerance. In addition, it is conservative in the use of laminate materials which is important when developing new matrix polymers or new fibres. On the other hand, the test does not simulate any practical situation; it is unlikely that a composite structure would be repetitively impacted in the same spot with increasing force with each blow. Moreover, interpretation of the RIIE test results requires both nondestructive (ultrasonic examination) and destructive (sectioning) to confirm the extent and type of damage that occurs with the change in stiffness.

5. Conclusions

Impact testing by repetitive impacts with increasing energy was studied and it was found that this technique does not discern changes in the type of damage with increasing cumulative impact energy. Instead, the changes in the impact response, notably stiffness, are the result of changes in the extent of damage. In the case of laminates based on a brittle thermoset matrix, 3501-6, there were distinct changes in stiffness that corresponded to the development of through-the-thickness damage and then to the extension of the

damage to the specimen edges. In the case of the thermoplastic matrix material, polyetheretherketone, the changes in stiffness were not as abrupt as for the thermoset but instead there was a gradual decline in stiffness. None the less, the damage progressed in the same manner; first through-the-thickness damage then extension of the damage to the specimen edges.

Static flexure testing of the 3501-6 matrix laminates resulted in the same changes in stiffness and extent of damage as observed in the dynamic tests. Static testing of the thermoplastic matrix laminates gave results somewhat different from the dynamic tests. These differences were attributed to the lower modulus thermoplastic laminates undergoing membrane deformation in the static tests and the greater time-dependent, viscoelastic nature of the thermoplastic compared to the thermoset.

References

1. N. J. JOHNSTON, "Toughened Composites", American Society for Testing and Materials, ASTM STP 937 (1987).
2. D. A. WYRICK and D. F. ADAMS, *J. Comp. Mater.* **22** (1988) 749.
3. K. STELLBRINK, in "Mechanical Characterization of Load Bearing Composite Laminates", edited by A. H. Cardon and G. Verchery (Elsevier Applied Science, London, 1984) p. 169.
4. P. ZOLLER, *Polym. Testing* **3** (1983) 197.
5. W. D. BASCOM, NASA Contractor Report 181965, "Fractography of Composite Delamination," NASA Langley Research Center, July 1990.
6. W. D. BASCOM, D. J. BOLL, J. C. WEIDNER and W. J. MURRI, *J. Mater. Sci.* **21** (1986) 2667.

Received 10 September
and accepted 19 November 1990